Unusual Strain Resulted from Interaction Between Permanent Magnets

V.I. Nizhankovskiy*

Institute of Low Temperature and Structure Research, Polish Academy of Sciences, Okólna 2, 50-422 Wroclaw, Poland

Detailed investigations of the properties essential for the interaction of permanent NdFeB magnets were performed at $T = 300$ and 77 K. Axial and radial magnetic field distribution, attracting force, and work are well described using a single-turn substitutional coil model. Strain resulting from the interaction of magnets was calculated and measured for the first time. Unexpected radial strain and additional negative change in the magnet volume were revealed in the experiment performed at $T = 77$ K. This additional change in the volume was proportional to the diminishing of the magnet free energy. A similar dependence was observed for the magnetostriction. It was concluded that any change in the magnetic free energy F_m is accompanied by the change in the elastic free energy $\delta F_e \approx 0.1\delta F_m$ at $T = 77$ K. At room temperature, δF_e is much smaller than δF_m.

topics: NdFeB magnets, elastic properties, magnetic properties

1. Introduction

Permanent magnets have a very wide spectrum of applications in different fields, from aerospace and industry to medicine and robotics [1]. In many applications, attractive or repulsive interaction of permanent magnets is used. Numerous theoretical and experimental investigations of this interaction were performed [2–4].

Of course, the interaction of permanent magnets should result in their deformation. Two contributions may be expected: the deformation due to the mechanical force and the magnetostriction. Until now, no such measurements have been done.

In the present work, we have investigated the deformation of a cylindrical NdFeB magnet as a function of distance from an identical permanent magnet (Fig. 1). Besides, we have determined the elastic parameters of NdFeB and measured its magnetostriction. Thus, it was possible to estimate the deformation from the mechanical force and the magnetostriction and compare estimations with the experiment. A very large qualitative and quantitative difference was observed, which correlates with the work done when the distance between the magnets is changed.

Before describing the experiment, it is necessary to give basic formulas for the magnetic field and force between the permanent magnets obtained in the assumption of uniform magnetization.

The axial and the radial components of the magnetic field of a current J flowing in a circle with radius a are (see §29, Problem 2 in [5])

$$B_z(z, r) = \frac{\mu_0}{4\pi} J \frac{2}{\sqrt{(a+r)^2 + z^2}}$$
$$\times \left[K(k) + \frac{a^2 - r^2 - z^2}{(a-r)^2 + z^2} E(k) \right], \qquad (1)$$

$$B_r(z, r) = \frac{\mu_0}{4\pi} J \frac{2z}{r\sqrt{(a+r)^2 + z^2}}$$
$$\times \left[-K(k) + \frac{a^2 + r^2 + z^2}{(a-r)^2 + z^2} E(k) \right], \qquad (2)$$

where $k^2 = 4ar/[(a+r)^2 + z^2]$, and $K(k)$ and $E(k)$ are complete elliptic integrals of the first kind and the second kind, i.e.,

$$K(k) = \int_0^{\pi/2} \frac{\mathrm{d}\theta}{\sqrt{1 - k^2 \sin^2(\theta)}},$$

$$E(k) = \int_0^{\pi/2} \mathrm{d}\theta \sqrt{1 - k^2 \sin^2(\theta)}. \qquad (3)$$

The free energy $\mathcal{F}$ of a current loop in an external magnetic field is

$$\mathcal{F} = J\Phi, \qquad (4)$$

where Φ is the magnetic flux of the external field through the current loop.

If $J = $ const, then the force acting on the current loop is (see §32 in [5])

$$F = J\frac{\partial\Phi}{\partial z}. \tag{5}$$

The axial magnetic field produced by a uniformly magnetized cylindrical permanent magnet is the same as that produced by a thin cylindrical coil and may be found by integration of (1) over the magnet length l

$$B_z(z,r) = \frac{\mu_0}{4\pi}M\int_0^l dy\ \frac{2}{\sqrt{(a+r)^2 + (z+y)^2}}$$
$$\times \left[K(k) + \frac{a^2 - r^2 - (z+y)^2}{(a-r)^2 + (z+y)^2}E(k)\right], \tag{6}$$

where M is the magnetization.

The radial component $B_r(z,r)$ is calculated by integration of (2) over the magnet length.

The magnetic flux

$$\Phi(z) = \int_0^a dr\ 2\pi r B_z(z,r), \tag{7}$$

and the attractive force between the magnets for $M = $ const is

$$F(z) = M\left[\Phi(z) - \Phi(z+l)\right]. \tag{8}$$

2. Experiment

Experiments were carried out using commercial NdFeB cylindrical magnets ($l = 5$ cm, $2a = 1.2$ cm).

Several measuring cells with a gradually increasing number of capacitor sensors were constructed.

Figure 1b shows the cell #3 equipped with five sensors. Flat sensors $C0$ and $C4$ were used for the axial strain measurement, and concentric sensors $C1, C2, C3$ — for the radial one. The upper end of the magnet was epoxy-glued to the 10 mm thick fibreglass washer.

Figure 1c shows the cell #5 equipped with six capacitive censors. In the middle of the magnet, a 5 mm thick fibreglass washer was epoxy-glued to mount the magnet in the measuring cell. Thus, the force from the upper movable magnet should result in the elongation of the top half of the fixed magnet and in the contraction of the bottom half. Figure 2 shows a photo of the elements of this measuring cell.

As the second electrode of all sensors, a magnet was used. Electrical contacts to the magnets were made by soldering a thin wire at a distance of 11 mm from the top of the magnet for cell #3 and in the middle of the magnet for cell #5.

Measuring cell #5 (Fig. 2) was made in the following way. In the beginning, concentric capacitive sensors and insulating spacers were glued into a housing with an internal diameter of 14.5 mm and an external diameter of 30 mm. The initial inner diameter of concentric capacitive sensors and insulating spacers was 11 mm. After that, the cell and the fibreglass washer were connected with fastening
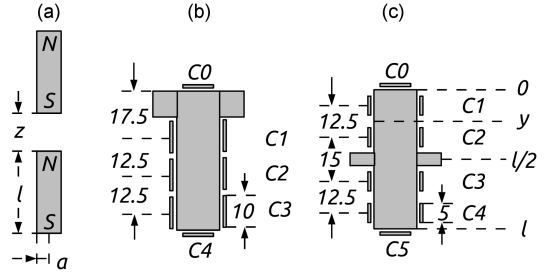

Fig. 1. Schematics of the experiment (a) and measuring cells of the lower fixed magnet: (b) cell #3, (c) cell #5. Dimensions are given in millimetres.
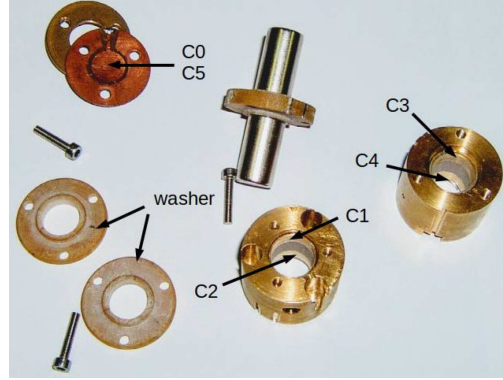

Fig. 2. Photo of elements of measuring cell #5.

screws made of non-magnetic stainless steel, and the inner diameter of the cell was increased to 12 mm so that the magnet entered it with little friction. Then the cell was disassembled, the washer and magnet were connected with a small amount of epoxy (the washer of cell #5 consisted of two parts), and the cell and magnet with the washer were assembled again until the epoxy polymerized. After that, the cell was disassembled and its inner diameter was increased to 12.5 mm.

Measuring cell #3 was made in a similar way.

Used technology should ensure good alignment of the magnet and concentric sensors.

The measuring cell and movable magnet with the force sensor were inserted into a closed thin-wall stainless steel tube filled with gaseous helium.

Strain and force were measured when the upper magnet was moved up from the lowest position $z = 0.2$ cm to $z > 9$ cm with a speed of about 0.07 cm/s using the rack and pinion type of linear actuator. Capacitance was measured by means of the AH 2500A bridge at a frequency of 1 kHz.

Force was measured with a PS 10K sensor, usable only at room temperature.

The Young modulus and Poisson's ratio were obtained from the results of the pulse ultrasonic measurements. LiNbO$_3$ transducers working in the longitudinal ($Y + 36°$ cut, $3 \times 3 \times 0.3$ mm^3 plate) and shear mode (X cut, $3 \times 4 \times 0.3$ mm^3 plate) were used.
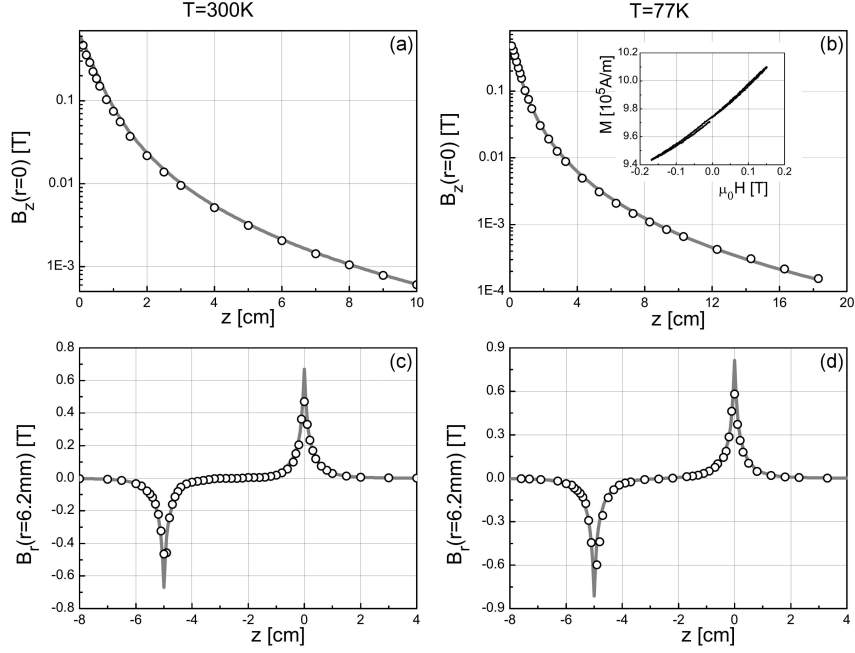
Fig. 3. Axial (B_z) and radial (B_r) magnetic field produced by NdFeB magnet measured at $T = 300$ and 77 K. Grey lines — theoretical dependencies calculated for $M = 9.73 \times 10^5$ A/m at $T = 300$ K and for $M = 1.18 \times 10^6$ A/m at $T = 77$ K. Inset in (b) shows the magnetization as a function of applied magnetic field measured at $T = 77$ K.

3. Results

3.1. Elastic properties

First, we checked the isotropy of the elastic properties of used NdFeB magnets. For this purpose, the longitudinal c_l and transverse c_t sound velocities were measured on the parallelepiped $2.4 \times 2 \times 1$ cm^3 magnet magnetized along the shortest dimension. The density of this magnet was $\rho = 7.405$ g/cm^3.

It was established that the transverse sound velocity ct is independent of the direction of propagation (upper index) and the direction of polarization (additional lower index) parallel ($\parallel$) or perpendicular ($\perp$) to the direction of the magnetization. Longitudinal sound velocity c_l was 2% lower along the direction of the magnetization than perpendicular to it, see Table I. Thus, the NdFeB magnet is almost isotropic.

Results obtained from measurements done with LiNbO$_3$ transducers glued to the ends of the cylindrical magnets of cells #3 and #5 are given in the lower line of Table I.

Higher values of sound velocities obtained with cylindrical magnets correlate with their higher density $\rho = 7.508$ g/cm^3.

Elastic constants, i.e., the Young modulus E and Poisson's ratio σ, were calculated from the equations (see Eq. (22.4) in [6])

$$c_l = \sqrt{\frac{E(1-\sigma)}{\rho(1+\sigma)(1-2\sigma)}}, \quad c_t = \sqrt{\frac{E}{2\rho(1+\sigma)}}. \quad (9)$$

TABLE I

Longitudinal and transverse sound velocities [km/s] measured with parallelepiped (upper line) and cylindrical NdFeB magnets at $T = 77$ K.

	$c_l^{\parallel}$	$c_l^{\perp}$	$c_t^{\parallel}$	$c_{t\parallel}^{\perp}$	$c_{t\perp}^{\perp}$
	6.20	6.33	3.58	3.59	3.59
#3	6.50	–	3.65	–	–
#5	6.49	–	3.64	–	–

TABLE II

Elastic properties of NdFeB magnet.

T [K]	E [GPa]	σ
300	224	0.244
77	254	0.270

Average results for magnets of cells #3 and #5 are given in Table II. It should be noted that values of the Young modulus are 1.6 times higher than obtained in [7] with a three-point bending test.

3.2. Magnetic properties

Figure 3a, b shows the dependence of the axial magnetic field on distance from the magnet. Figure 3c, d shows the dependence of the radial magnetic field measured at a distance of 6.2 mm from the magnet axis (the magnet is located
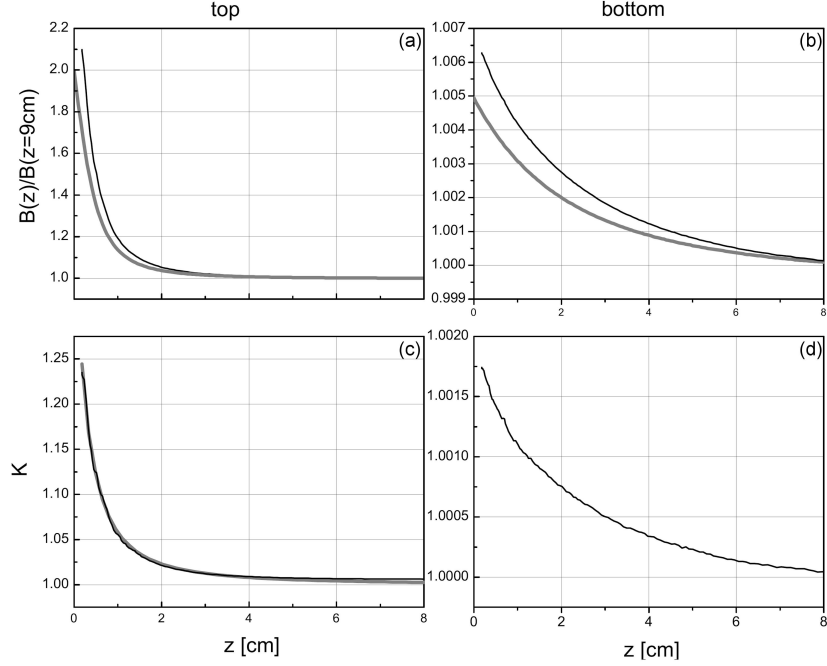
Fig. 4. Dependence of the magnetic field at the upper end (a) and at the lower end (b) of fixed magnet on the distance between the magnets measured at $T = 77$ K. Black lines — experiment, grey lines — calculations for $M =$ const. (c) Black line — experimental dependence of the correction coefficient at the upper end of the fixed magnet, wide grey line — approximation. (d) Correction coefficient at the lower end of the fixed magnet.

from -5 to 0 cm). These measurements were done at room and liquid nitrogen temperatures by points with a small 1×1 mm^2 Hall sensor. Grey lines in Fig. 3a, b are the fitting of the experimental points to (6) with resulting magnetization $M(300$ K$) = 9.73 \times 10^5$ A/m and $M(77$ K$) = 1.18 \times 10^6$ A/m. The same values of magnetization were used in calculations of the radial magnetic field (Fig. 3c, d).

In the inset of Fig. 3b, the field dependence of magnetization is shown. This result was obtained at $T = 77$ K with a small cylindrical magnet ($\varnothing 3.9$ mm, $l = 4$ mm) using a VSM magnetometer [8]. This dependence was fitted to $M(B\,[T]) \approx M(0)(1 + 0.22B + 0.2B^2)$.

The increase in the magnetization with an applied magnetic field results in a larger than the simple sum value of the magnetic field between the magnets at $T = 77$ K.

Figure 4a shows a continuous record of the magnetic field at the upper end of the fixed magnet at the distance to the movable magnet made at $T = 77$ K. If $M =$ const, then there should be $B(0)/B(\infty) = 2$ and $B(0)/B(9$ cm$) < 2$.

Black line in Fig. 4c shows the coefficient K by which the calculated for $M =$ const magnetic field should be multiplied in order to obtain the experimental dependence $B(z)/B(9$ cm$)$ shown in Fig. 4a. Grey line in Fig. 4c is the approximation $K(z) = 0.059(z + 0.48)^{-1.79}$ (z is given in cm).

It follows from Fig. 4c that at $T = 77$ K, approaching magnets have up to 10% larger magnetization at the near ends.

Correction for the field diminishes with distance and may be neglected at the lower end of the fixed magnet (Fig. 4d).

Measurements of the attractive force were made at room temperature.

The black line in Fig. 5a shows the continuous record of attractive force as a function of distance between the magnets. The wide grey line was calculated according to (8) for $M = 9.73 \times 10^5$ A/m. Good agreement was obtained for three orders of magnitude change in magnetic field and attractive force.

From the analysis of theoretical equations, it follows that the ratio of force (see (8)) to the axial field (see (6)) should have a local minimum at $z \approx 0.6\,a$. The depth of this minimum is very sensitive to the magnetization, which allows for the best determination of its value. A comparison of the experimental and theoretical dependencies $F(z)/B_z(z)$ is given in the inset in Fig. 5a.

3.3. Dilatometric measurements

To calculate the change in the magnet dimensions from the measured capacitance of the sensors, we used the following formulas obtained from the electrostatics

$$\frac{\delta r}{r} = \frac{h}{1.8}\left(\frac{1}{C_0} - \frac{1}{C}\right), \quad \delta l = \frac{a^2}{3.6}\left(\frac{1}{C_0} - \frac{1}{C}\right),$$
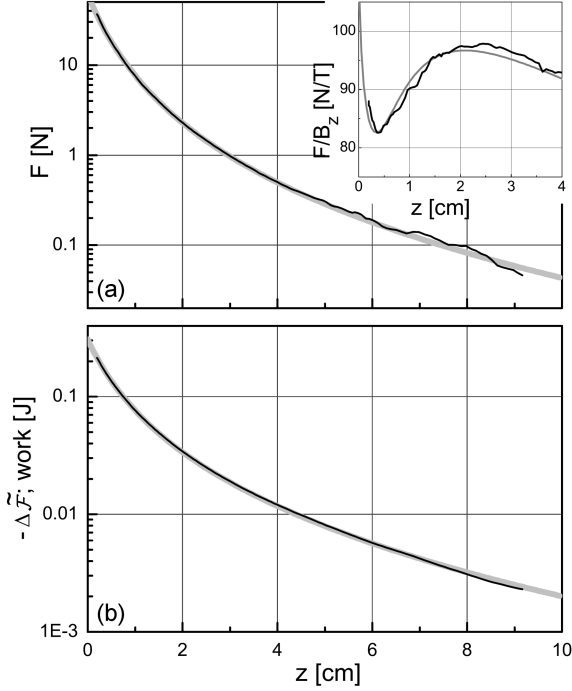
$$(10)$$

Fig. 5. (a) Attractive force as a function of distance between NdFeB magnets measured at $T = 300$ K. Inset: dependence ratio of force to the axial field on distance. Black lines — experiment, grey lines — calculations for $M = 9.73 \times 10^5$ A/m. (b) Black line — work calculated by integration of the experimental $F(z)$ dependence. Grey line — change in the free energy of the magnet calculated for $M = 9.73 \times 10^5$ A/m.

where h is the width of the concentric sensor, a — magnet radius, C_0 — capacitance at the largest distance between the magnets (h and a are in cm, capacitance — in pF).

To ensure the necessary temperature stability, dilatometric measurements were done at $T = 77$ K. A magnetic field was produced by a copper coil cooled by liquid nitrogen.

Results of the magnetostriction measurements are shown in Fig. 6. Scattering of the experimental points for the radial magnetostriction obtained with wide sensors $C1$–$C3$ of cell #3 (Fig. 6a) is much smaller than that obtained with narrow sensors $C1$–$C4$ of cell #5 (Fig. 6b). This means that the size of inhomogeneities is smaller than 1 cm. Perfect overlap of the results for the axial magnetostriction obtained with sensors $C0$ and $C5$ of cell #5 (Fig. 6d) confirms this conclusion.

The axial magnetostriction of cell #3 is shown in Fig. 6. The striction measured with sensor $C4$ is eight times larger than the striction measured with sensor $C0$. From this ratio, it follows that the magnet is fixed at a distance of 5.5 mm from the top, which seems quite reasonable. Total relative axial magnetostriction is $\delta l/l = (\delta l_0 + \delta l_4)/l$.

In Fig. 6, the gradual diminishing of the slope of the strain vs applied magnetic field dependences is visible for $B_z > 0$. Obtained experimental results for the magnetostriction of cell #3 were fitted to the following expressions (magnetic field is in Tesla)

$B_z < 0$:

$$\frac{\delta r}{r} = 3.1 \times 10^{-5} B_z, \quad \frac{\delta l}{l} = -4.6 \times 10^{-5} B_z, \tag{11}$$

$B_z > 0$:

$$\frac{\delta r}{r} = 1.85 \times 10^{-5} B_z^{0.88}, \quad \frac{\delta l}{l} = -2.65 \times 10^{-5} B_z^{0.88}. \tag{12}$$

The same values of parameters well describe magnetostriction measured with cell #5.

The target results are presented in Fig. 7, where the deformations of the magnets fixed in cells #3 and #5 as a function of distance to the movable magnet are shown.

Absolutely unexpected are negative values of the radial strain obtained near the lower end of the magnet (sensor $C3$ of cell #3 and sensor $C4$ of cell #5). Indeed, radial magnetostriction is positive (Fig. 6), and the attractive force between the magnets should result in a contraction of the length and an expansion of the diameter.

3.4. Calculations

Data for the elastic properties, the attractive force, and the magnetostriction allow us to evaluate the supposed strain of the fixed magnet resulting from the influence of the movable magnet.

Calculations of the magnetostrictive contribution are rather simple. At first, the mean value of the external magnetic field at a distance y from the upper end of the fixed magnet is determined as $B_z(z+y) = \Phi(z+y)/(\pi a^2)$. Then, this value is multiplied by coefficient $K(z+y)$ (Fig. 4c). After that, the radial $\delta r/r$ and axial $\delta l/l$ contributions are found using corresponding coefficients (12) by integration over y. For example, for sensor $C1$ of cell #3

$$\frac{\delta r_1}{r(z)} = \frac{1.85 \times 10^{-5}}{0.01} \int_{0.0125}^{0.0225} dy \left[K(z+y) B_z(z+y) \right]^{0.88}, \tag{13}$$

where 0.01 in the denominator is the width of the concentric capacitor sensor in m.

Calculation of the attraction force contribution is much more complicated because it requires solving a partial differential equation with definite boundary conditions. Even in the simple case of the gravitational field, the boundary conditions could not be satisfied in some places (§7, Problem 1 in [6]).

We have estimated strain due to the attractive force without solving any differential equation in the following way.
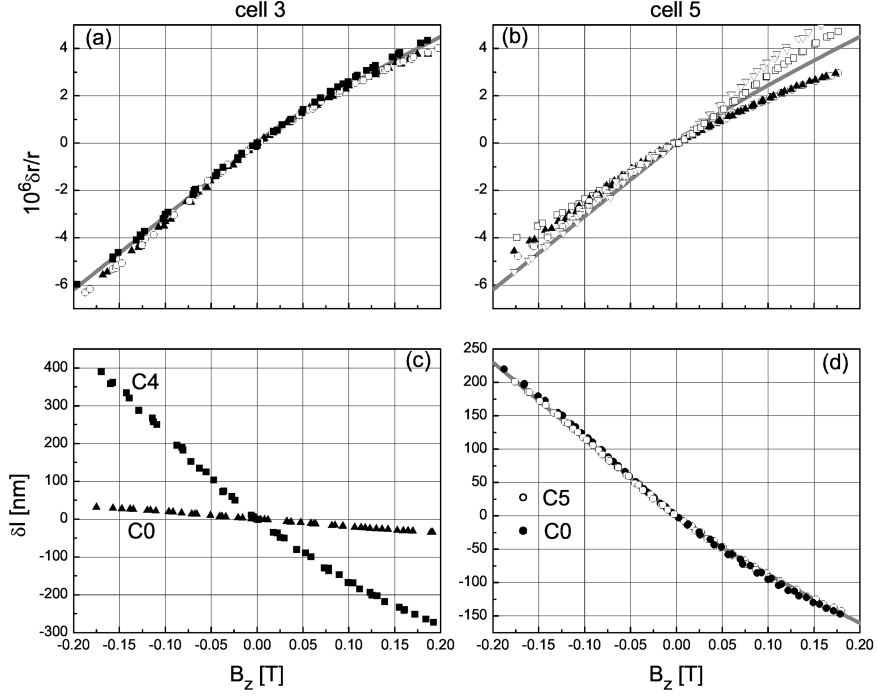
Fig. 6. Magnetostriction measured at $T = 77$ K; (a, c) cell #3; (b, d) cell #5. Different symbols correspond to different capacitive sensors. Grey lines show approximation of expressions (11) and (12).
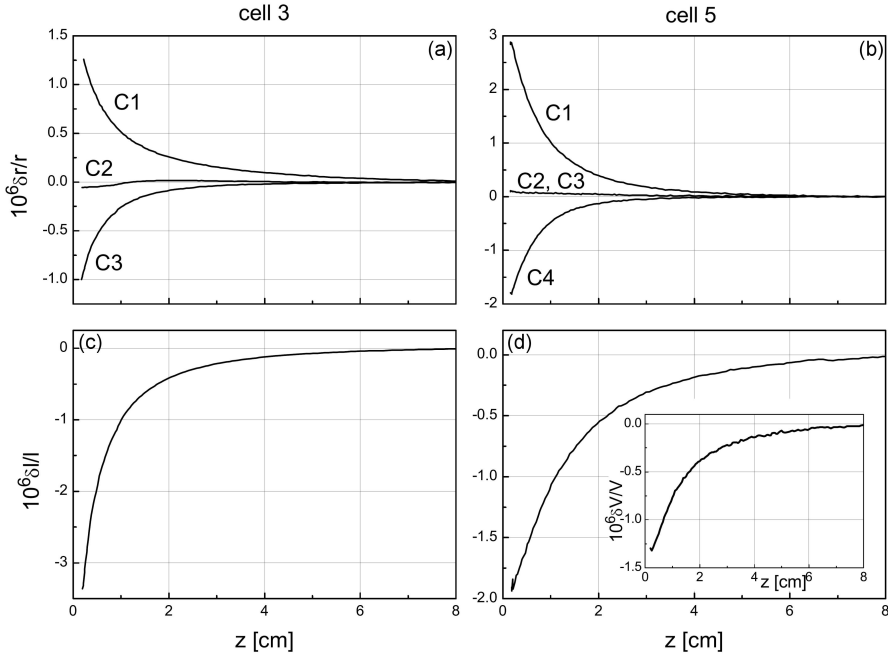

Fig. 7. Radial $\delta r/r$ and axial $\delta l/l$ strain of the fixed magnet as a function of distance z from the movable magnet measured at $T = 77$ K; (a, c) cell #3; (b, d) cell #5. Inset in (d) shows change in volume.

Let us consider cell #5 (Fig. 1c). The unmovable magnet is fixed in the measuring cell with the washer glued halfway along the magnet length l. Force acting on the section positioned at the distance y in the upper part of the magnet is $F(z + y) = M[\Phi(z+y) - \Phi(z+y+l/2)]$. The pressure is $p(z, y) = F(z+y)/(\pi a^2)$, the axial strain is $\delta l/l(z, y) = p(z, y)/E$, and the radial strain is $\delta r/r(z, y) = -\sigma \, \delta l/l(z, y)$.

Then, corrections for the magnetization and magnetic field were taken into account, and an integral similar to (13) was calculated.
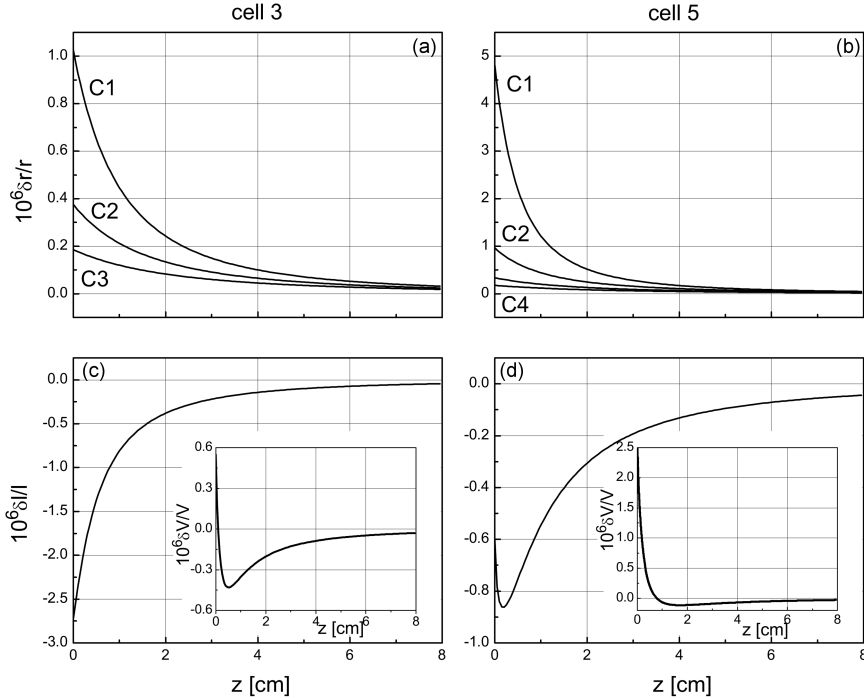
Fig. 8. Calculated for $M(77\ \text{K}) = 1.18 \times 10^6$ A/m radial $\delta r/r$ and axial $\delta l/l$ strain of the fixed magnet as a function of distance z from the movable magnet; (a, c) cell #3; (b, d) cell #5. Insets in panels (c) and (d) show changes in volume.

Analogous equations determine strain in the lower part of the magnet.

Due to neglecting the boundary conditions, $\delta r/r(z,y)$ has a jump at $y = l/2$. Fortunately, the magnetostrictive contribution to the radial strain is an order of magnitude larger than the contribution of the attractive force, and this jump does not exceed 3% of $\delta r/r$ at this position.

Using the calculated $\delta r/r(z,y)$ dependence, the mean value of radial change was determined as $\delta r/r(z) = l^{-1} \int_0^l \mathrm{d}y\ \delta r/r(z,y)$. The change in the volume is $\delta V/V(z) = 2\,\delta r/r(z) + \delta l/l(z)$.

The calculated total strain and change in volume are shown in Fig. 8. As one can see, the radial strain $\delta r/r$ is always positive, and the axial strain $\delta l/l$ is negative.

It should be pointed out that corrections for magnetic field and magnetization rapidly decreased with distance and had a small (below 10%) influence on the results of calculations.

Of course, the number of radial sensors is too small to obtain the real shape of the magnet deformation from the experimental data. Nevertheless, we have estimated the change in the magnet volume for cell #5. At first, data $\delta r_i/r$ $(i = 1, \ldots, 4)$ were fitted by the third-order polynomial $P(y)$, and the mean value of radial change was determined as $\delta r/r = l^{-1} \int_0^l \mathrm{d}y\ P(y)$. The obtained change in the volume $\delta V/V = 2\,\delta r/r + \delta l/l$ is shown in the inset in Fig. 7d.

4. Discussion

As we have seen, the magnetic field and force of a permanent magnet are perfectly described by a thin substitutional coil with current $J = l\,M$, where l is the magnet length, and M is its magnetization (Figs. 3 and 5).

It is necessary to explain why corrections for the magnetization and magnetic field obtained at $T = 77$ K and resulting from the dependence of magnetization on the magnetic field (inset in Fig. 3b) have no effect on the attractive force measured at $T = 300$ K.

NdFeB undergoes the spin-reorientation transition at $T_{SRT} = 130$ K. Its magnetic properties below and above T_{SRT} are quite different. In particular, the slope of M vs B dependence at $T = 77$ K is four times larger than at $T = 300$ K [9]. Correspondingly, corrections to the magnetization and magnetic field at room temperature are four times smaller. The correction to the attractive force is 16 times weaker and could not be detected.

Let us discuss the thermodynamics of the problem.

The free energy of a single-turn coil itself (without a source of current) is $\mathcal{F} = LJ^2/2$.

The self-induction L of a thin coil is (see §33, Problem 6 in [5])

$$L = \frac{\mu_0}{4\pi} \frac{8\pi a^2}{l^2} \int_0^l \int_0^\pi \frac{\mathrm{d}z\ \mathrm{d}\theta\ (l-z)\cos(\theta)}{\sqrt{z^2 + 4a^2 \sin^2(\theta/2)}}. \quad (14)$$

Inserting $a = 0.6$ cm, $l = 5$ cm, one gets $L = 2.573$ nH. Thus, the free energy of each substitutional coil for $M = 10^6$ A/m is 3.22 J, and the total initial free energy is $\mathcal{F}_i = 6.44$ J.

When two magnets are in contact, the length of the substitutional coil is doubled, its inductance diminishes to 1.351 nH, and the final free energy is $\mathcal{F}_f = 6.76$ J.

Thus, the free energy of two substitutional coils increases by $\Delta\mathcal{F} = 0.32$ J.

Exactly the same result may be obtained in another way.

The free energy of two coils is $\mathcal{F} = L_1 J_1^2/2 + L_2 J_2^2/2 + L_{12} J_1 J_2$, where L_{12} is the mutual inductance. In the geometry of the experiment

$$L_{12}(z) = \frac{\mu_0}{4\pi} \frac{2\pi a^2}{l^2} \int_0^l \int_z^{z+l} \int_0^{2\pi} \frac{dz_1\, dz_2\, d\theta\, \cos(\theta)}{\sqrt{(z_1-z_2)^2 + 4a^2 \sin^2(\theta/2)}},$$

(15)

where z is the distance between the coils. This equation is a generalization of (14).

When two coils are in contact, $L_{12}(0) = 0.13$ nH and $\Delta\mathcal{F} = 0.32$ J.

In the thermodynamic sense, a permanent magnet is equivalent to a system consisting of a coil and a current source. A change in the free energy $\tilde{\mathcal{F}}$ of this system has the opposite sign to the change in the free energy of a coil itself $\Delta\tilde{\mathcal{F}} = -\Delta\mathcal{F}$ (see §32 in [5] and [10]).

Thus, the free energy of two attracted magnets is 5% smaller than the free energy of separate magnets.

It is of interest to compare the dependence of the free energy determined by the mutual inductance of the substitutional coils on the distance between these coils with the work produced by converging magnets $\int_\infty^z dz\, F(z)$.

This comparison is shown in Fig. 5b. Wide grey line is the change in the free energy calculated as $\Delta\tilde{\mathcal{F}}(z) = -L_{12}(z)J^2$, where the current $J = l M = 0.05 \times 9.73 \times 10^5 = 4.86 \times 10^4$ A corresponds to the magnetization M at room temperature. The mechanical work (black line) was calculated from the experimental $F(z)$ dependence measured at room temperature (Fig. 5a). Because the maximum value of the z-coordinate was not infinite (9.3 cm), the result of integration was shifted up by 2.3 mJ.

Both dependencies coincide. This means that the work produced by converging magnets is equal to the decrease in their magnetic free energy $\tilde{\mathcal{F}}$.

Let us discuss the results of the dilatometric measurements.

The observed strain (Fig. 7) is very different from the calculated strain (Fig. 8). The most striking difference is the negative radial strain near the bottom of the magnet observed in the experiment, but impossible according to the calculations taking into account the mechanical force and magnetostriction (Fig. 8). Besides, observed axial contraction is noticeably larger than calculated strain.
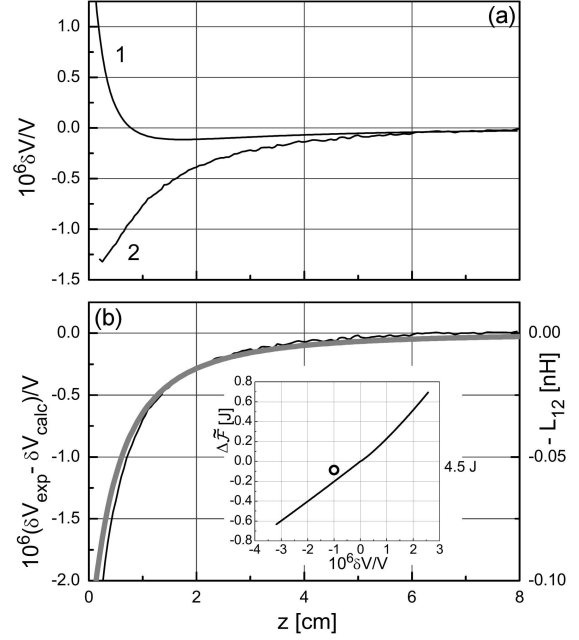

Fig. 9. (a) Calculated (1) and measured (2) change in the magnet volume cell #5 at $T = 77$ K. (b) Difference between the experimental and calculated dependencies of $\delta V/V$ (black line) and the mutual inductance (grey line). Inset: change in the magnet free energy as a function of the change in the volume. Black line shows the results of the magnetostriction measurements, and circle corresponds to the additional contribution.

Sensors $C1$ and $C4$ of cell #5 (Fig. 1c) are placed symmetrically near the ends of the magnet. Absolute values of measured strain (Fig. 7b) have the same order, but magnetic field produced by the movable magnet at the top of the fixed magnet is two orders of magnitude higher than at the bottom.

Negative radial strain near the bottom of the magnet could not be ascribed to the possible radial shift of the magnet relative to the concentric sensor. Indeed, in this case, the capacitance of the sensor is given by equation (see §3, Problem 7 in [5])

$$C = 2\pi\varepsilon_0 h \left[\coth^{-1}\left(\frac{r_1^2 + r_2^2 - x^2}{2r_1 r_2} \right) \right]^{-1},$$

(16)

where r_1, r_2 and h are the sensor dimensions, and x is the axes shift.

From (16) it follows that the capacitance and, therefore, the seeming strain should increase with the axes shift. Calculations made for sensor $C4$ of cell #5 resulted in $\delta r/r \approx 0.65\,(x/a)^2$.

We must conclude that an additional contribution to the strain should exist.

Figure 9a shows a comparison of the calculated (curve 1) and obtained from the experiment with cell #5 (curve 2) change in the magnet volume. In Fig. 9b, the additional contribution is plotted and compared with the dependence of the mutual inductance $-L_{12}$ of the substitutional coils on the

distance between the magnets. Both dependencies almost coincide. This means that the additional contribution to the change in the volume is proportional to the change in the magnet free energy $\Delta\tilde{\mathcal{F}}(z) = -L_{12}(z)J^2/2$ (we consider only one magnet). For a quantitative description of this dependence, it suffices to take data for one value of $z = 0.72$ cm, where $\delta V_{add}/V(z) = -1 \times 10^{-6}$, $L_{12}(z) = 0.05$ nH (Fig. 9b) and $\Delta\tilde{\mathcal{F}}(z) = -0.087$ J.

In the case of magnetostriction (Fig. 6), the change in the volume is proportional to the corresponding change in the free energy $\Delta\tilde{\mathcal{F}}(H) = BM_s/2$, where B is the applied magnetic field and M_s is the magnetic moment of the sample. The inset in Fig. 9b shows the change in the free energy as a function of the change in the magnet volume. The line corresponds to the magnetostriction calculated using (11) and (12) and taking into account the dependence of magnetization on magnetic field. The obtained curve may be well-fitted by a parabola. Zero on the y-axis corresponds to the initial free energy of magnet $\tilde{\mathcal{F}}_0 = LJ^2/2 = 4.5$ J. The circle near this line shows the result obtained above for the additional contribution.

From the inset in Fig. 9b, it follows that any change in the magnet free energy is accompanied by a change in the magnet volume and unexpected experimental strain (Fig. 7) results from the thermodynamics.

There is no simple correspondence between the free energy of the magnet and its elastic free energy.

As it is well known, as temperature decreases from $T > T_C$ with the transition to the ferromagnetic state, a spontaneous magnetostriction is observed. For $Nd_2Fe_{14}B$ from experimental results shown in Fig. 3 of work [11], we have estimated spontaneous strains at $T = 77$ K along and perpendicular to the magnetic moment as $\lambda_\parallel \approx 2.5 \times 10^{-3}$ and $\lambda_\perp \approx 5.5 \times 10^{-3}$.

The corresponding density of elastic free energy may be calculated from the general expression

$$F_e = \mu\left(\varepsilon_x^2 + \varepsilon_y^2 + \varepsilon_z^2\right) + \tfrac{1}{2}\lambda\left(\varepsilon_x + \varepsilon_y + \varepsilon_z\right)^2, \qquad (17)$$

where ε_i are the strains, and μ and λ are the Lamè coefficients (see Eq. (4.1) in [6]).

As we have seen, the elastic properties of NdFeB are almost isotropic, hence the Lamè coefficients may be obtained using equations

$$\mu = \frac{E}{2(1+\sigma)}, \qquad \lambda = \frac{\sigma E}{(1+\sigma)(1-2\sigma)}, \qquad (18)$$

where E is Young's modulus and σ is Poisson's ratio (see §5 in [6]).

Using experimental data for E and σ given in Table II, we obtained $\mu = 100$ GPa, $\lambda = 117$ GPa, and also the estimated elastic energy $F_e \approx 17.4$ J/cm^3. This value is 22 times larger than the density of the magnetic free energy $F_m = \tilde{\mathcal{F}}/V \approx 0.8$ J/cm^3.

An opposite relation was obtained from the results of the magnetostriction measurements.

Results of calculations δF_e and δF_m from the magnetostriction measurements of NdFeB magnet.

B_z [T]	$\delta r/r$ ($\times 10^6$)	$\delta l/l$ ($\times 10^6$)	$\delta V/V$ ($\times 10^6$)	δF_e [J/cm^3]	δF_m [J/cm^3]
-0.2	-6.2	9.2	-3.2	-0.014	-0.113
0.2	4.5	-6.4	2.6	0.011	0.124

Change in the elastic free energy was calculated using equation

$$\delta F_e = 2\mu\left[2\lambda_\perp\left(\delta r/r\right) + \lambda_\parallel\left(\delta l/l\right)\right]$$
$$+\lambda\left(2\lambda_\perp + \lambda_\parallel\right)\left[2\left(\delta r/r\right) + \left(\delta l/l\right)\right], \qquad (19)$$

which follows from (17). Change in the magnetic free energy $\delta F_m = \Delta\tilde{\mathcal{F}}/V$.

The results of the calculations are summarised in Table III.

From Table III, it follows that in the case of the magnetostriction, the change in the elastic free energy is $8 \div 11$ times smaller than the change in the magnetic free energy.

Let us consider the additional negative change in the fixed magnet volume resulting from the interaction with the movable magnet. The corresponding change in the elastic free energy may be roughly estimated under the assumption $\delta r/r = \delta l/l = \frac{1}{3}\delta V_{add}/V$. Taking from the above $\delta V_{add}/V(z = 0.72$ cm$) = -1 \times 10^{-6}$ and using (19), we have obtained $\delta F_e = -2.48 \times 10^{-3}$ J/cm^3. This value is 6.3 times smaller than $\delta F_m = \Delta\tilde{\mathcal{F}}/V = -1.55 \times 10^{-2}$ J/cm^3. This result is in a rough agreement with the magnetostriction data.

Thus, any change in the magnetic free energy F_m is accompanied by the change in the elastic free energy $\delta F_e \approx 0.1\delta F_m$ at $T = 77$ K (i.e., below the spin-reorientation transition). At room temperature, δF_e should be much smaller than δF_m because, within the experimental precision, the work produced by converging magnets is equal to the decrease in their magnetic free energy, see Fig. 6.

Our observations are in agreement with the ideas of a very old work [12], in which the need to take into account the mutual influence of magnetic and elastic properties was pointed out.

5. Conclusions

In the present work, the essential physical properties of permanent magnets — magnetic field distribution, magnetization, elastic properties, magnetostriction — were investigated. The results of these investigations were used to predict the strain of the NdFeB magnet as a function of the distance between two attracting magnets.

The attractive force measured at $T = 300$ K and calculated work are in agreement with the theoretical description in which magnets are substituted by single-layer coils.

The deformation of the magnet fixed in the cell equipped with several capacitor sensors was measured at $T = 77$ K. Unexpected negative strain at the bottom end of the magnet was observed and ascribed to the additional contribution.

The additional contribution to the change in the magnet volume was proportional to the change in the magnet free energy. The same proportionality takes place in the case of the magnetostriction.

The relation between the magnetic free energy and the elastic free energy was discussed.

Acknowledgments

References

[1] J.M.D. Coey, *J. Magn. Magn. Mater.* **248**, 441 (2002).

[2] S. Agashe, D.P. Arnold, *J. Phys. D Appl. Phys.* **41**, 105001 (2008).

[3] D. Vokoun, M. Beleggia, L. Heller, P. Šittner, *J. Magn. Magn. Mater.* **321**, 3758 (2009).

[4] R. Ravaud, G. Lemarquand, S. Babic, V. Lemarquand, C. Akyel, *IEEE Trans. Magn.* **46**, 3585 (2010).

[5] L.D. Landau, E.M. Lifshitz, *Electrodynamics of Continuous Media*, 2nd ed., Pergamon Press, 1984.

[6] L.D. Landau, E.M. Lifshitz, *Theory of Elasticity*, 2nd ed., Pergamon Press, 1975.

[7] P. Vedrine, P. Tixador, Y. Brunet, J.C. Bobo, A. Fevrier, A. Leriche, *Cryogenics* **31**, 51 (1991).

[8] V.I. Nizhankovskii, L.B. Lugansky, *Meas. Sci. Technol.* **18**, 1533 (2007).

[9] G. Le Bec, J. Chavanne, C. Benabderrahmane, in: *Proc. of 23rd Particle Accelerator Conf.*, Vancouver 2009, p. 327.

[10] R. Howard, *Found. Phys.* **10**, 109 (1980).

[11] H. Fujii, H. Nagata, Y. Uwatoko, T. Okamoto, H. Yamamoyo, M. Sagawa, *J. Magn. Magn. Mater.* **70**, 331 (1987).

[12] W.F. Brown Jr., *Revs. Modern Phys.* **25**, 131 (1953).